

Cite this: *Chem. Sci.*, 2023, 14, 284

All publication charges for this article have been paid for by the Royal Society of Chemistry

Received 28th September 2022
Accepted 28th November 2022

DOI: 10.1039/d2sc05409d
rsc.li/chemical-science

Introduction

Nitrogen-doping (N-doping) of polycyclic aromatic hydrocarbons (PAHs) is an efficient strategy to tailor the optical and electrochemical properties of parent PAHs.^{1,2} Similar to N-doped graphene^{3,4} the type of nitrogen species in PAHs could also be distinguished as pyridinic nitrogen,⁵ pyrrolic nitrogen,⁶ and graphitic nitrogen⁷ depending on the site of the nitrogen atom (Fig. 1). The type of doped nitrogen atom greatly influences the properties of N-doped PAHs. While pyridinic nitrogen affords more electron-deficient PAHs, the other two give rise to more electron-rich PAHs due to an increase in the number of π -electrons. Furthermore, different from pyrrolic nitrogen that involves a five-membered ring, graphitic nitrogen can be seen as a direct replacement of a carbon atom in an aromatic six-membered ring by nitrogen, thereby adding one electron to the respective π -system. Interest in synthesizing PAHs doped with a specific type of nitrogen arises from the debate over the properties and reactivity of N-doped graphene with different types of doped nitrogen.^{8–13} Synthesis of N-doped PAHs with well-defined sizes and specific concentrations and positions of nitrogen atoms provides an opportunity to accurately investigate the effects of N-doping on graphitic carbon. However, N-

doped PAHs reported in the literature have principally been limited to those containing pyridinic and pyrrolic nitrogen atoms which could be easily obtained by replacing benzene rings with pyridine or pyrrole.¹ Few examples of graphitic N-doped PAHs have been reported, which required multiple-step syntheses.^{7,14–19} This scarcity of PAHs with graphitic nitrogen might be due to the lack of a synthetic strategy that can form six-membered rings around a nitrogen atom. One of the few examples of such methods has recently been reported by Lindner and co-workers,¹⁸ where a one-pot Buchwald–Hartwig cross-coupling/direct arylation reaction^{20–22} was used to synthesize a luminescent N-doped PAH for OLEDs. However, there have been no attempts at the development of a versatile synthetic method to access a series of graphitic N-doped PAHs.

Here we introduce a synthetic method for graphitic N-doped PAHs and investigate their properties. Thus, we designed 15-*b*-azatribenzo[*de,hi,op*]tetracene (Scheme 1) as naphthalene-

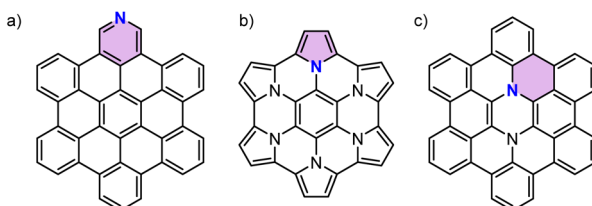


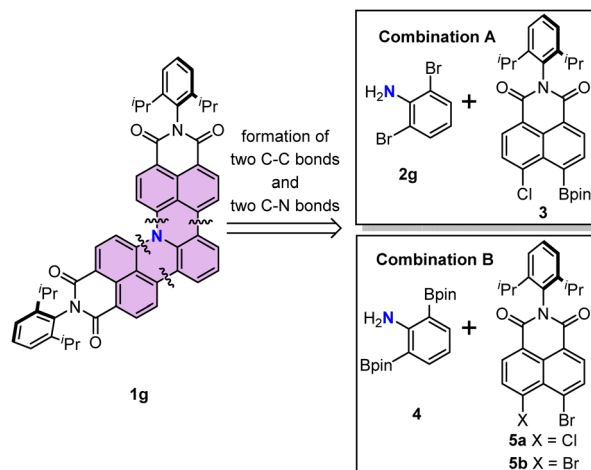
Fig. 1 Chemical structures of the reported N-doped PAHs with different types of doped nitrogen atoms. For each structure an aromatic ring containing a specific type of doped nitrogen atom is highlighted by color. Substituents are omitted for clarity. (a) Pyridinic N-doped PAH.⁵ (b) Pyrrolic N-doped PAH.⁶ (c) Graphitic N-doped PAH.⁷

^aUniversität Würzburg, Institut für Organische Chemie, Am Hubland, Würzburg 97074, Germany. E-mail: wuerthner@uni-wuerzburg.de

^bUniversität Würzburg, Center for Nanosystems Chemistry (CNC), Theodor-Boerner-Weg, Würzburg 97074, Germany

† Electronic supplementary information (ESI) available: Experimental and calculation details. CCDC 2190556, 2190559–2190563. For ESI and crystallographic data in CIF or other electronic format see DOI: <https://doi.org/10.1039/d2sc05409d>





Scheme 1 Retrosynthetic analysis and design of building blocks. The structure of *15b*-azatribenzol[*de,hi,op*]tetracene is highlighted in color.

bridged aniline and developed a cascade reaction for [3 + 3] naphtho-annulation of halogenated aniline. In order to stabilize the electron-rich N-doped π -scaffold imide substituents are installed to lower the oxidation potential. The optimized reaction conditions yielded a series of N-doped PAHs containing graphitic nitrogen. Furthermore, pyridinic or pyrrolic nitrogen could also be installed using substrates already containing such nitrogen. The synthesized N-doped PAHs exhibited high stability under ambient conditions and high fluorescence quantum yields. Thus, we anticipate that the new class of N-doped imide-functionalized PAHs provides an important extension of the structural and functional space of so-far explored imide-functionalized PAHs and nanographenes.^{23,24}

Results and discussion

We first describe the retrosynthetic analysis for the target molecule **1g**. This molecule possesses one aniline and two

naphthalimide moieties. Thus, **1g** might be obtained from naphthalimide and an aniline derivative through formation of two C-C bonds and two C-N bonds (Scheme 1). We chose the Suzuki–Miyaura cross-coupling reaction for the formation of the two C-C bonds, because it has been developed as the most widely used method to construct a C-C bond.^{25,26} The Buchwald–Hartwig amination reaction or nucleophilic aromatic substitution reaction is a potential method to construct the desired C-N bond.^{27,28} Therefore, we decided to use readily available 2,6-dibromoaniline (**2g**) as the aniline coupling partner and *N*-(2,6-diisopropylphenyl)-5-chloro-naphthalene-1,8-dicarboximide-4-boronic acid (pinacol) ester (**3**) as a boron reagent to optimize the reaction conditions (Scheme 1, combination A). An alternative combination of aniline-2,6-diboronic acid bis(pinacol)ester (**4**) and *N*-(2,6-diisopropylphenyl)-4,5-dihalo-naphthalene-1,8-dicarboximide (**5**) (Scheme 1 combination B)^{29,30} was also examined.

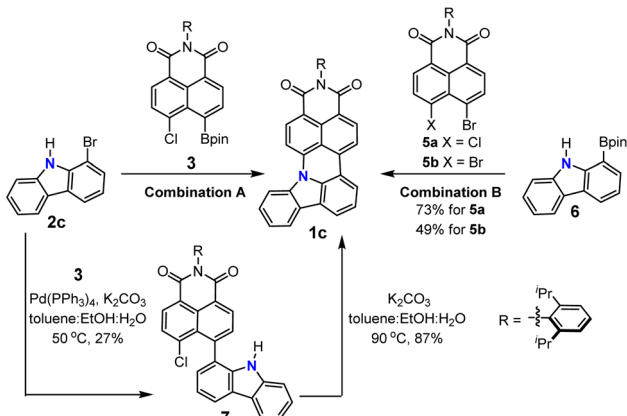
After preparation of building block **3** (details of synthesis described in the ESI†), the mono-annulation reaction with **2c** was used as a model reaction to optimize the reaction conditions (Table 1 and Scheme 2). Considering the requirement of the formation of the C-C bond and C-N bond, we evaluated a dual catalyst system for both the Suzuki–Miyaura coupling and Buchwald–Hartwig amination reactions, *i.e.* $Pd(PPh_3)_4$ for C-C bond formation and $Pd_2(dbu)_3/(t-Bu)_3P$ for amination (entries 1–3). Among the three tested conditions, only $Pd_2(dbu)_3/Pd(OAc)_2$ with $P(t-Bu)_3/P(Cy)_3$ as the ligand and NaO^tBu as the base in toluene could afford the desired product in 50% yield (entry 2). Because the yield was only moderate for the dual ligand system, we hypothesized that the combination of Suzuki coupling and intramolecular S_NAr cascade reactions might give higher yields. To our delight, reactions using four commonly used catalysts for Suzuki coupling and a base for both Suzuki coupling and S_NAr reactions all could afford the desired product (entries 4–7), with the reaction using $Pd(PPh_3)_4/K_2CO_3$ showing the best performance with 77% yield (entry 7). Subsequently, the influence of base was explored as well (entries 7–9). Among the used bases, K_2CO_3 is the most suitable one for

Table 1 Optimization of the reaction conditions for the Suzuki coupling/intramolecular S_NAr cascade reaction^a

	Catalyst	Ligand	Base	Solvent	Yield ^b
1	$Pd_2(dbu)_3/Pd(PPh_3)_4$	$P(t-Bu)_3$	NaO^tBu	Toluene	—
2	$Pd_2(dbu)_3/Pd(OAc)_2$	$P(t-Bu)_3/P(Cy)_3$	NaO^tBu	Toluene	50
3	Xphos Pd G2/Pd($PPh_3)_4$	—	NaO^tBu	Dioxane	—
4	$Pd(dppf)Cl_2$	—	K_2CO_3	Toluene : EtOH : H_2O	75
5	$Pd(OAc)_2$	Sphos	K_3PO_4	n -Butanol : H_2O	25
6	Xphos Pd G2	Xphos	K_2CO_3	Toluene : EtOH : H_2O	61
7	$Pd(PPh_3)_4$	—	K_2CO_3	Toluene : EtOH : H_2O	77
8	$Pd(PPh_3)_4$	—	Na_2CO_3	Toluene : EtOH : H_2O	35
9	$Pd(PPh_3)_4$	—	Cs_2CO_3	Toluene : EtOH : H_2O	60
10	$Pd(PPh_3)_4$	—	K_2CO_3	Toluene	11
11 ^c	$Pd(PPh_3)_4$	—	K_2CO_3	Toluene : EtOH : H_2O	73
12 ^d	$Pd(PPh_3)_4$	—	K_2CO_3	Toluene : EtOH : H_2O	49

^a **2c** (40 μ mol, 1.0 equiv.), **3** (2.0 equiv.), catalyst (0.10 equiv.), ligand (0.20 equiv.), base (3.0 equiv.), solvent (toluene : EtOH : H_2O 5 : 2 : 1, n -butanol : H_2O 2 : 1), 90 °C, 16 h. ^b Isolated yield. ^c **6** and **5a** as substrates. ^d **6** and **5b** as substrates. SPhos: 2-dicyclohexylphosphino-2',6'-dimethoxybiphenyl, XPhos: 2-dicyclohexylphosphino-2',4',6'-triisopropylbiphenyl, PCy₃: tricyclohexylphosphine, $P(t-Bu)_3$: trif(tert-butyl)phosphine, dppf: 1,1'-bis(diphenylphosphino)ferrocene, dba: dibenzylideneacetone.





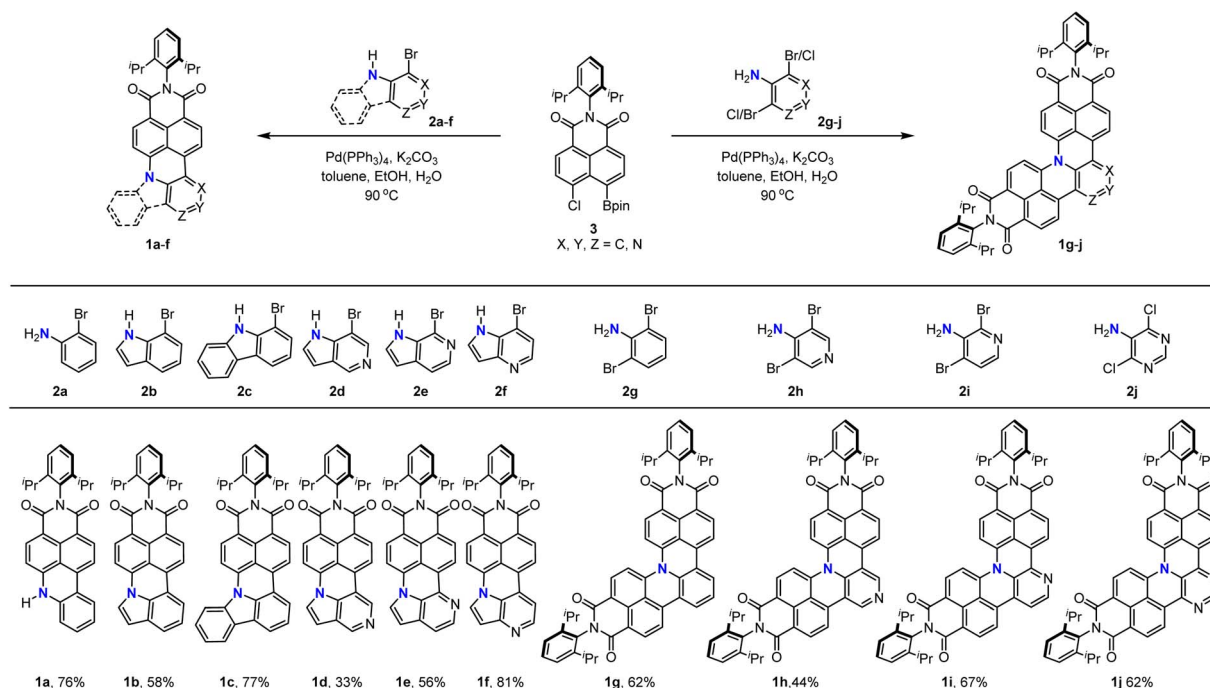
Scheme 2 Reaction pathway towards 1c.

this cascade reaction; weaker or stronger bases such as Na_2CO_3 or Cs_2CO_3 both lead to lower yields. Furthermore, the necessity of water and ethanol as co-solvents in this reaction was proved by the control reaction using toluene as the sole solvent, which afforded the desired product only in 11% yield (entry 10). We further applied the optimized conditions to combination B (Scheme 2), which uses boronic ester substituted aniline as the coupling partner. A comparable result was obtained when 6 and 5a were applied as the substrates (entry 11); however, the yield was decreased to 49% when 5b was used as the coupling partner (entry 12).

The proposed reaction pathway of this cascade reaction is illustrated in Scheme 2. Because the applied reaction conditions are those for a typical Suzuki coupling reaction and not suitable for Buchwald–Hartwig amination, the first step of this

cascade should be a common Suzuki coupling reaction to form the C–C bond. This could also be proved by a control experiment using the conditions in Table 1 entry 7 but at lower temperature and a shorter reaction time (50 °C for 4 hours), where the intermediate 7 could be isolated (the relatively low yield of 7 is due to the high reactivity of 7, which could convert to the final product 1c fast under the reaction conditions) and its structure was unambiguously confirmed by ^1H and ^{13}C NMR spectroscopy as well as high-resolution mass spectrometry. Thus, the second step of this cascade reaction should be a nucleophilic aromatic substitution reaction which benefits from the electron-withdrawing character of dicarboximide to increase the ability of the chloride substituent as the leaving group and also stabilize the Meisenheimer complex.³¹ This hypothesis was substantiated by the almost quantitative transformation of 7 to 1c under basic conditions in a toluene, ethanol, and water mixture without any palladium catalyst. These results support our reaction pathway for the N-doped PAHs *via* a Suzuki coupling/intramolecular $\text{S}_{\text{N}}\text{Ar}$ cascade reaction.

With the optimized reaction conditions in hand, we turned our attention to the substrate scope of this cascade annulation (Scheme 3). 2-Bromoaniline 2a, 7-bromoindole 2b, and 1-bromo-9H-carbazole 2c all could be coupled with 3 to afford the corresponding N-doped PAHs 1a–c in 58–77% yield. Moreover, azaindole with nitrogen at a different position could also be applied to this reaction, furnishing the products 1d–f in moderate to high yields. Finally, we used these reaction conditions for the synthesis of double-annulated products. N-doped PAHs 1g–i could be isolated in 44–67% yields when 2,6-dibromoaniline 2g, 3,5-dibromo-4-pyridinamine 2h, and 2,4-dibromo-3-pyridinamine 2i were applied. Encouraged by the



Scheme 3 Substrate scope of the palladium-catalyzed cascade reaction for the synthesis of N-doped PAHs.



above excellent results, we then extended this catalytic system to 5-amino-4,6-dichloropyrimidine **2j**, which is a difficult substrate for the Suzuki coupling reaction due to coordination of the substrate onto the palladium catalyst and the lower reactivity of chlorine. The desired product **1j** could be isolated in 62% yield, demonstrating the wide substrate scope of this synthetic method.

All N-doped PAHs were fully characterized by ^1H and ^{13}C NMR spectroscopy as well as high-resolution mass spectrometry (ESI ‡). Furthermore, single crystals of **1c** and **1g–j** suitable for X-ray analysis were grown by slow diffusion of hexane or methanol into their dichloromethane or toluene solutions and thus their molecular structures could be unambiguously confirmed. N-doped PAHs **1c** and **1j** crystallize in a monoclinic crystal system with $P2_1/n$ and $P2_1/c$ space groups, respectively. Other bisimides **1g**, **1h**, and **1i** crystallize in a triclinic crystal system with a $P\bar{1}$ space group for **1g** and **1i** and $P\bar{1}$ space group for **1h**. Mono-annulated compound **1c** is almost planar with a small torsion angle (5° , Fig. 2a). The solid-state packing arrangement of **1c** (Fig. 3a) is characterized by tightly stacked head-to-tail antiparallel dimers with average π - π distances of approximately 3.51 Å. Twofold-annulated compounds **1g–j** are nonplanar and possess a [4]helicene backbone with average torsion angles of 26.5° , 24.4° , 25.9° , and 22.6° in the inner helix, respectively (Fig. 2b–e). The Gibbs activation energies of enantiomerization ($\Delta G^\ddagger(T)$) of **1g–i** were calculated at the B3LYP/6-31G(d) level of theory to be 15.4, 15.1, and 15.2 kcal mol $^{-1}$, respectively, while the $\Delta G^\ddagger(T)$ of **1j** was significantly larger with 19.7 kcal mol $^{-1}$. All these calculated activation energies were much larger than that of unsubstituted [4]helicene (4.5 kcal mol $^{-1}$ calculated at the B3LYP/6-31G(d) level of theory).

Unlike the planar structure of mono-annulated compounds, which could form dimer packing motifs through π - π interactions (Fig. 3a), double-annulated compounds **1g–j** did not show direct π - π interaction between molecules; instead one or two molecules of toluene stacked in between. Both **1g** and **1i** have almost the same packing structure, stacks of centrosymmetric head-to-head dimers comprising *M*- and *P*-configuration isomers (Fig. 3b and d). The chiral crystal structure of **1h** was solved as racemic twins, where **1h** and toluene solvate formed alternating columnar stacks with average π - π distances of 3.67

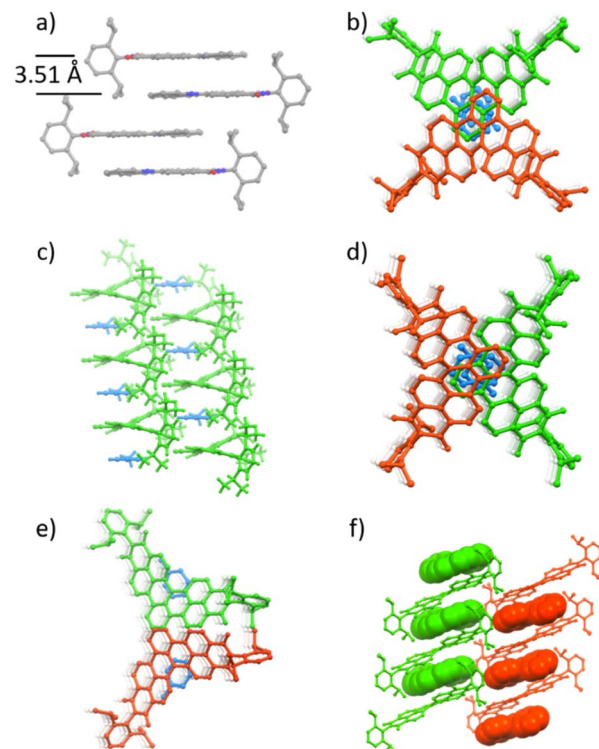


Fig. 3 Packing arrangement of (a) **1c**, (b) **1g**, (c) **1h**, (d) **1i**, (e) **1j**, and (f) **1g**/[4]helicene. Blue: toluene, green: *M* configuration, and red: *P* configuration. Hydrogen omitted for clarity. For (f) guest [4]helicene is depicted by a space filling model.

Å (Fig. 3c). There is only one molecule of **1h** in the asymmetric unit of this chiral crystal with the $P\bar{1}$ space group, which aligns this [4]azahelicene unit-containing **1h** without any other symmetry operation than translational symmetry in the solid-state, giving this molecule the potential to be applied to nonlinear optical technologies (Fig. 3c).³² Bisimide **1j** formed alternating columnar stacks with toluene, where two adjacent stacks are separated by a mirror plane (Fig. 3e). The packing structure of double-annulated compounds inspired us to explore their potential for the growth of co-crystals of these compounds with suitable guest molecules. Indeed, we succeeded in growing co-crystals of **1g** with [4]helicene (Fig. 3f).

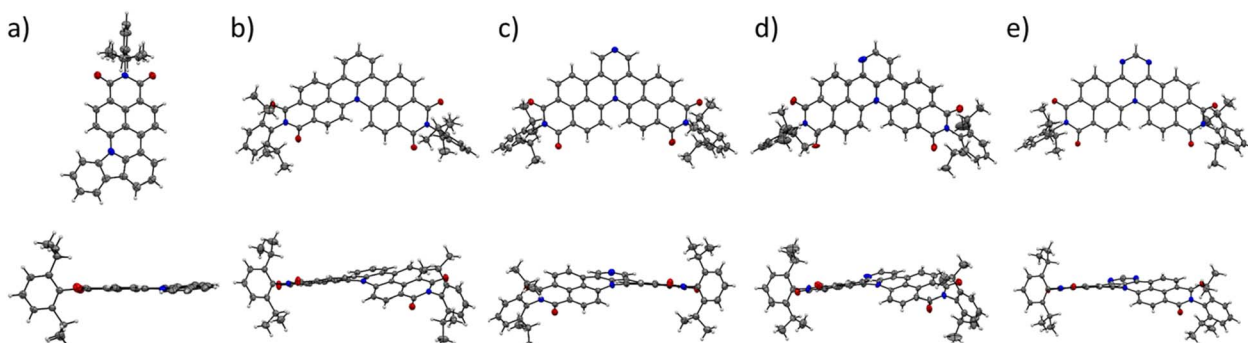


Fig. 2 Solid-state molecular structures of (a) **1c**, (b) **1g**, (c) **1h**, (d) **1i**, and (e) **1j** determined by single-crystal X-ray diffraction analysis. Thermal ellipsoids are set at 50% probability.



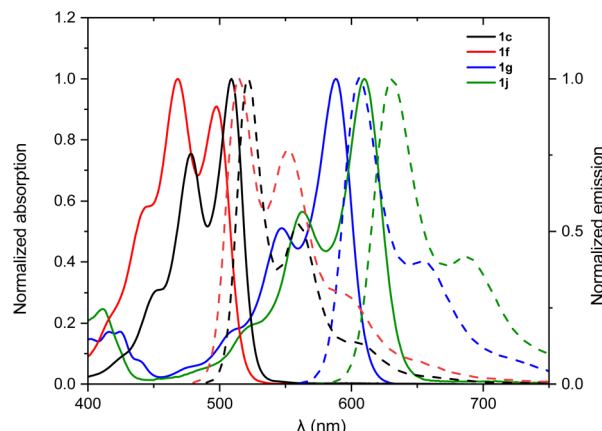


Fig. 4 Absorption (solid line) and emission (dotted line) spectra of **1c**, **1f**, **1g**, and **1j** (chloroform solution, $c \sim 4 \times 10^{-6}$ M for UV-vis, OD ~ 0.05 for fluorescence at 293 K).

Bisimide **1g** formed a columnar stack with [4]helicene with the same configuration in the crystal structure, indicating the ability of this molecule to host guest molecules of the same chirality.

The optical properties of the new N-doped PAHs **1a–j** were investigated by UV/vis absorption spectroscopy and fluorescence emission spectroscopy in chloroform solutions at room temperature (Fig. 4, S1–S3† and Table 2). All N-doped PAHs show absorption bands with clearly resolved vibronic structures and small Stokes shifts ($490\text{--}720\text{ cm}^{-1}$), indicating relatively small changes in their geometry in ground and excited states. Mono-annulated compounds **1a–f** exhibit similar absorption and emission spectral features with perylene monoimides (PMIs).³³ Interestingly, mono-annulated compounds are also highly fluorescent with fluorescence quantum yields close to unity, thereby even surpassing the parent PMI (Table 2). **1a–c** show very similar absorption (longest wavelength absorption maxima are located at 505 nm) and emission spectra (longest wavelength emission maxima are located at 522 nm) with different extinction coefficients due to different sizes of the

aromatic π -system (Fig. S1†). The lowest energy absorption maxima of **1d–f** are at 486, 504, and 497 nm, respectively, which are slightly hypsochromically shifted to the lowest energy absorption maxima of **1a–c** (505–509 nm). This is in good accordance with their electrochemical energy gaps (*vide infra*). Fluorescence lifetime (FL) for mono-annulated compounds ranges from 5.93 to 7.73 ns. Double-annulated compounds **1g–j** show a well-resolved $S_0\text{--}S_1$ transition at $\lambda_{\text{abs}} = 588, 560, 598$, and 610 nm, respectively, with a shoulder located in the higher energy region and a mirror-image fluorescence with λ_{em} of 607, 578, 617, and 631 nm, respectively. Pyrimidine-containing **1j** exhibits the largest values for λ_{abs} and λ_{em} among these ten N-doped PAHs. The fluorescence quantum yields of these double-annulated compounds are 23–84%, which are smaller compared to those of the mono-annulated products. We attribute these low quantum yields to the enhanced intersystem crossing caused by their non-planar [4]helicene backbone.³⁴ The FLs of **1i** (6.49 ns) and **1j** (6.47 ns) are similar to those of mono-annulated compounds; however the FLs of **1g** (3.14 ns) and **1h** (1.74 ns) are much smaller compared to those of mono-annulated compounds. The experimental absorption spectra of the newly synthesized N-doped PAHs are in good agreement with their TDDFT calculated spectra (Fig. S8–S10†). Overall, the absorption maxima of these ten N-doped PAHs could be changed from 486 nm (**1d**) to 610 nm (**1j**), demonstrating the capability of N-doping to adjust optical properties of PAHs.

The redox properties of newly synthesized N-doped PAHs **1b–j** were investigated by cyclic and square wave voltammetry (**1a** was insoluble for this investigation). The measurements were performed in dichloromethane at room temperature using tetrabutylammonium hexafluorophosphate as electrolyte and the ferrocenium/ferrocene (Fc^+/Fc) redox couple as the internal standard. The voltammograms are displayed in Fig. S7† and the electronic properties are summarized in Table S2.† All measured mono-annulated compounds **1b–f** showed one reduction and one oxidation process and double-annulated compounds **1g–j** showed two reduction and two oxidation processes. The HOMO and LUMO energy levels of these N-doped PAHs were calculated based on their first oxidation/

Table 2 Optical properties of the N-doped PAHs

	λ_{abs}^a (nm)	λ_{em}^b (nm)	ε [$\text{M}^{-1} \text{ cm}^{-1}$]	ϕ_{fl}^c [%]	E_{HOMO}^d [eV]	E_{LUMO}^d [eV]
1a	505	524	21 400	94	—	—
1b	508	521	35 700	99	-5.97	-3.40
1c	509	522	44 300	99	-5.95	-3.35
1d	486	500	31 200	99	-6.09	-3.47
1e	504	519	33 300	99	-6.12	-3.56
1f	497	515	25 000	99	-6.20	-3.58
1g	588	607	70 000	38	-5.93	-3.66
1h	560	578	59 500	23	-6.09	-3.74
1i	598	617	65 900	84	-6.01	-3.81
1j	610	631	63 400	64	-6.09	-3.96
PMI^e	507	545	31 000	85	-6.10	-3.69

^a Measured in chloroform ($c \sim 4.0 \times 10^{-6}$ M). ^b Measured in chloroform (OD ~ 0.05). ^c Determined using the absolute quantum yield method. ^d Calculated using the equations $E_{\text{LUMO}} = -[E(M/M^-) + 5.15\text{ eV}]$ and $E_{\text{HOMO}} = -[E(M/M^+) + 5.15\text{ eV}]$, assuming that the energy level of Fc^+/Fc with respect to the vacuum level is -5.15 eV . ^e Data from ref. 32 and 34.



reduction waves and are summarized in Table 2. While the first reduction processes of all nine measured molecules were reversible, the first oxidation process was reversible only for **1c** and **1g–1j**. Other mono-annulated compounds **1b** and **1d–f** showed pseudo-reversible or irreversible first oxidation processes presumably due to the unstable α -double bond of the (aza)indole subunit. The HOMO energy levels of these N-doped PAHs are very similar to those of PMI;³⁵ however, mono-annulated products show much higher LUMO energy levels compared with PMI, reflecting the electron-donating character of the doped graphitic/pyrrolic nitrogen. Azaindole annulated products **1d–f** (−3.47 to −3.58 eV) exhibited lower LUMO energy levels compared with indole and carbazole annulated products **1b** (−3.40 eV) and **1c** (−3.35 eV) due to the electron-withdrawing character of azaindole. The LUMO energy levels of **1g–j** were −3.66, −3.74, −3.81, and −3.96 eV, respectively, which are much lower compared with those of mono-annulated products due to the second dicarboximide. The order of the LUMO energy level was **1j** < **1i** < **1g**, which could be explained by the fact that pyridine and pyrimidine are much more electron deficient compared to benzene. The LUMO energy levels of these N-doped PAHs clearly demonstrated the effect of different types of doped nitrogen atoms on the LUMO energy level.

Conclusions

In summary, a new Suzuki coupling/intramolecular S_NAr cascade reaction was developed for rationally designed building blocks. Ten N-doped PAHs were efficiently synthesized by our approach in moderate to good yields, including four double-annulated compounds. This cascade reaction could be applied to form PAHs containing different types of nitrogen, such as graphitic, pyrrolic and pyridinic, demonstrating the versatility of this cascade reaction. The crystal structures of **1c** and **1g–j** were determined by single crystal X-ray diffraction analysis and their structures were unambiguously confirmed, where the torsion angles of these N-doped PAHs range from *ca.* 5° (mono-annulated products) to *ca.* 25° (double-annulated products). The optical properties and electrochemical properties of these N-doped PAHs were systematically investigated. Mono-annulated products **1a–f** exhibited high fluorescence quantum yields (94–99%) and small Stokes shifts (490–720 cm^{−1}). The absorption maxima of annulated products varied over 125 nm (0.52 eV), from 486 nm to 610 nm and the LUMO energy levels were between −3.35 eV and −3.96 eV, demonstrating the usefulness of N-doping to adjust optical and electronic properties. Furthermore, this cascade reaction might also be applicable for the synthesis of larger sized N-doped PAHs and would expand the scope of available N-doped PAHs.

Experimental methods

General procedure

2a–f (40.0 μ mol, 1.00 equiv.), compound **3** (80.0 μ mol, 2.00 equiv.), Pd(PPh₃)₄ (4.00 μ mol, 0.100 equiv.), and potassium carbonate (0.120 mmol, 3.00 equiv.) were charged in a 15 mL Schlenk tube under an argon atmosphere. Then 0.8 mL

toluene–EtOH–H₂O (5:2:1) was added into the flask *via* a syringe. The reaction mixture was heated at 90 °C under intense stirring and an argon atmosphere overnight. After cooling to room temperature, the reaction mixture was diluted with dichloromethane, washed with water and brine, dried over anhydride sodium sulfate, and filtered. After removal of solvent, the crude product was purified by column chromatography on silica-gel and precipitation from dichloromethane/cyclohexane to afford the product. For the synthesis of double-annulated products **2g–j** (40.0 μ mol, 1.00 equiv.), compound **3** (0.160 mmol, 4.00 equiv.), Pd(PPh₃)₄ (8.00 μ mol, 0.200 equiv.), and potassium carbonate (0.240 mmol, 6.00 equiv.) were applied.

Data availability

All experimental procedures and spectroscopic data can be found in the ESI.†

Author contributions

Xiaoqi Tian: investigation, methodology, writing. Kazutaka Shoyama: single crystal X-ray analysis writing, supervision. Frank Würthner: conceptualization, writing, supervision, funding acquisition.

Conflicts of interest

There are no conflicts of interest to declare.

Acknowledgements

We thank the Deutsche Forschungsgemeinschaft (DFG, German Research Foundation) for financial support (grant no. WU 317/20-2). We thank the Alexander von Humboldt Foundation for a postdoctoral stipend for Xiaoqi Tian. We acknowledge DESY (Hamburg, Germany), a member of the Helmholtz Association HGF, for providing experimental facilities at PETRA III under P11 proposal no. I-20211168. We thank Carolin Scheitl and Claudia Höbartner for sharing measurement time under P11 proposal no. I-20211108. We thank Dr Eva Crosas for assistance in using beamline P11.

Notes and references

- 1 A. Borissov, Y. K. Maurya, L. Moshniaha, W. S. Wong, M. Zyla-Karwowska and M. Stępień, *Chem. Rev.*, 2022, **122**, 565–788.
- 2 M. Hirai, N. Tanaka, M. Sakai and S. Yamaguchi, *Chem. Rev.*, 2019, **119**, 8291–8331.
- 3 X. Wang, G. Sun, P. Routh, D. H. Kim, W. Huang and P. Chen, *Chem. Soc. Rev.*, 2014, **43**, 7067–7098.
- 4 H. Wang, T. Maiyalagan and X. Wang, *ACS Catal.*, 2012, **2**, 781–794.
- 5 A. Graczyk, F. A. Murphy, D. Nolan, V. Fernandez-Moreira, N. J. Lundin, C. M. Fitchett and S. M. Draper, *Dalton Trans.*, 2012, **41**, 7746–7754.

6 M. Takase, T. Narita, W. Fujita, M. S. Asano, T. Nishinaga, H. Benten, K. Yoza and K. Müllen, *J. Am. Chem. Soc.*, 2013, **135**, 8031–8040.

7 X. Y. Wang, M. Richter, Y. He, J. Bjork, A. Riss, R. Rajesh, M. Garnica, F. Hennersdorf, J. J. Weigand, A. Narita, R. Berger, X. Feng, W. Auwarter, J. V. Barth, C. A. Palma and K. Müllen, *Nat. Commun.*, 2017, **8**, 1948.

8 D. Usachov, O. Vilkov, A. Gruneis, D. Haberer, A. Fedorov, V. K. Adamchuk, A. B. Preobrajenski, P. Dudin, A. Barinov, M. Oehzelt, C. Laubschat and D. V. Vyalikh, *Nano Lett.*, 2011, **11**, 5401–5407.

9 M. Skorupska, A. Ilnicka and J. P. Lukaszewicz, *Sci. Rep.*, 2021, **11**, 23970.

10 Z. Zhang, L. Yu, Y. Tu, R. Chen, L. Wu, J. Zhu and D. Deng, *Cell Rep. Phys. Sci.*, 2020, **1**, 100145.

11 D. Guo, R. Shibuya, C. Akiba, S. Saji, T. Kondo and J. Nakamura, *Science*, 2016, **351**, 361–365.

12 X. Cui, S. Yang, X. Yan, J. Leng, S. Shuang, P. M. Ajayan and Z. Zhang, *Adv. Funct. Mater.*, 2016, **26**, 5708–5717.

13 W. Ding, Z. Wei, S. Chen, X. Qi, T. Yang, J. Hu, D. Wang, L. J. Wan, S. F. Alvi and L. Li, *Angew. Chem., Int. Ed.*, 2013, **52**, 11755–11759.

14 E. Hamzehpoor and D. F. Perepichka, *Angew. Chem., Int. Ed.*, 2020, **59**, 9977–9981.

15 D. Sakamaki, D. Kumano, E. Yashima and S. Seki, *Chem. Commun.*, 2015, **51**, 17237–17240.

16 Y. Zagranjarski, A. Skabev, Y. Ma, K. Müllen and C. Li, *Org. Chem. Front.*, 2016, **3**, 1520–1523.

17 G. Zhu, Y. Song, Q. Zhang, W. Ding, X. Chen, Y. Wang and G. Zhang, *Org. Chem. Front.*, 2021, **8**, 727–735.

18 K. Bartkowski, P. Z. Crocomo, M. Kochman, D. Kumar, A. Kubas, P. Data and M. Lindner, *Chem. Sci.*, 2022, **13**, 10119–10128.

19 N. Hammer, T. E. Shubina, J. P. Gisselbrecht, F. Hampel and M. Kivala, *J. Org. Chem.*, 2015, **80**, 2418–2424.

20 L. Ackermann, R. Vicente and A. R. Kapdi, *Angew. Chem., Int. Ed.*, 2009, **48**, 9792–9826.

21 J. Wencel-Delord, T. Droke, F. Liu and F. Glorius, *Chem. Soc. Rev.*, 2011, **40**, 4740–4761.

22 T. Gensch, M. N. Hopkinson, F. Glorius and J. Wencel-Delord, *Chem. Soc. Rev.*, 2016, **45**, 2900–2936.

23 W. Jiang and Z. Wang, *J. Am. Chem. Soc.*, 2022, **144**, 14976–14991.

24 S. R. Peurifoy, T. J. Sisto, F. Ng, M. L. Steigerwald, R. Chen and C. Nuckolls, *Chem. Rec.*, 2019, **19**, 1050–1061.

25 N. Miyaura, K. Yamada and A. Suzuki, *Tetrahedron Lett.*, 1979, **36**, 3437–3440.

26 N. Miyaura and A. Suzuki, *Chem. Rev.*, 1995, **95**, 2457–2483.

27 J. F. Hartwig, *Angew. Chem., Int. Ed.*, 1998, **37**, 2046–2067.

28 S. Rohrbach, A. J. Smith, J. H. Pang, D. L. Poole, T. Tuttle, S. Chiba and J. A. Murphy, *Angew. Chem., Int. Ed.*, 2019, **58**, 16368–16388.

29 S. Seifert, K. Shoyama, D. Schmidt and F. Würthner, *Angew. Chem., Int. Ed.*, 2016, **55**, 6390–6395.

30 K. Shoyama, M. Mahl, S. Seifert and F. Würthner, *J. Org. Chem.*, 2018, **83**, 5339–5346.

31 F. Terrier, *Modern Nucleophilic Aromatic Substitution*, Wiley-VCH, 2013, e-book ISBN: 9783527656141.

32 B. B. Ivanova and M. Spiteller, *J. Phys. Chem. A*, 2010, **114**, 5099–5103.

33 S. Seifert, D. Schmidt and F. Würthner, *Org. Chem. Front.*, 2016, **3**, 1435–1442.

34 K. Nagarajan, A. R. Mallia, K. Muraleedharan and M. Hariharan, *Chem. Sci.*, 2017, **8**, 1776–1782.

35 J. Cremer, E. Mena-Osteritz, N. G. Pschierer, K. Müllen and P. Bäuerle, *Org. Biomol. Chem.*, 2005, **3**, 985–995.

